MOLECULAR PHYSICS, 1991, VOL. 73, NO. 2, 439–461

Head–tail asymmetry and ferroelectricity in uniaxial liquid crystals. Model calculations†

By F. BISCARINI‡ and C. ZANNONI
Dipartimento di Chimica Fisica ed Inorganica,
Universita', Viale Risorgimento, 4, 40136 Bologna, Italy

C. CHICCOLI and P. PASINI
INFN Sez. di Bologna and CNAF, Viale Ercolani, 8, 40138 Bologna, Italy

(*Received 16 August 1990; accepted 19 November 1990*)

We have studied in detail a simple model system with first- and second-rank interactions first examined many years ago by Krieger and James with mean field theory and used more recently as a prototype for bowlic and ferroelectric liquid crystals. We have investigated the model applying Monte Carlo simulations and two-site cluster theory and obtained its phase diagram. The existence of a ferroelectric liquid crystal phase region in this non-chiral system is confirmed also going beyond mean field theory. We also report short and long-range order parameters of first- and second-rank as a function of temperature for various ratios of the discriminating to non-discriminating interaction.

1. Introduction

Ferroelectric low molar mass [1] and polymeric liquid crystals [2] have become extremely interesting both for their fundamental properties and for their applicability in fast-switching electro-optic devices [3]. The only liquid crystals of this type that have been prepared and studied to date are, to our knowledge, chiral smectic C phases. There are, however, no reasons of principle to exclude other kinds of liquid crystal ferroelectric phases [4] and it is interesting to develop simple molecular models that try to find out the key ingredients that could give a ferroelectric liquid crystal. After all also the existence of chiral smectic C ferroelectrics had been predicted before they were actually synthesized. On a different ground it is curious enough that the contribution of polar interactions be normally neglected even though one of the first theories put forward on the structure of liquid crystals, due to Born [5], attributed the forces responsible for liquid crystal orientational ordering to dipolar forces. This hypothesis was later proved unsatisfactory as a general ordering mechanism, because no macroscopic dipole ordering is observed in nematics and, even more stringently, because apolar nematics were synthesized [6, 7]. Indeed such a great variety of different liquid crystals has now been prepared [8] that the hypothesis of collective ordering effects being due to a combination of different interactions both steric and attractive [9] rather than to a single ubiquitous one has become a very plausible proposition. On the other hand, although dipoles may not determine the existence of an ordered phase,

† A preliminary version of this work has been presented at the International Discussion Meeting on Relaxation in Complex Systems, Heraklion, 1990.

‡ Present address: Institute of Molecular Biology and Department of Chemistry, University of Oregon, Eugene, Oregon 97403-1229, USA.

0026-8976/91 $3.00

they are nevertheless present in the great majority of nematogens and they will produce some effect [10–17]. On an even more general basis, it is important to introduce a simple way of characterizing the dissymetry between head and tail existing in most liquid crystal molecules, and indeed in a number of elongated mesogens, e.g. in the popular alkyl cyano biphenyls, we have a chain on one end (the tail T, say) and a different group at the other end (the head H, say). Another prominent example is in ordered membrane bilayers, where the distinction between the polar head and the aliphatic chain is essential to the formation of the bilayer itself [18]. This is particularly relevant now also for columnar mesophases, because of the synthesis of classes of intrinsically asymmetric molecules, like those giving rise to pyramidic or bowlic liquid crystals [19, 20]. These mesogen have a cone shaped structure realized, for example, with a tribenzocyclononene [21, 22] or tetraphenyl [23] macrocyle with chains attached. In general terms we could describe the non-equivalence of head and tail of two parts of a molecule by means of shape multipoles [24] a concept relating to a systematic analysis of the mass or repulsive centres distribution [25] formally analogous to the more conventional analysis of charge distributions in electric multipoles. From this standpoint bowl-shaped molecules have a shape dipole as well as having an electric dipole. It is apparent that to treat liquid crystals made with these kind of molecules we need a model potential with first rank as well as second rank contributions. We can try to do this by introducing not a lot of very detailed and possibly 'realistic' terms, which would be on one hand overambitious and on the other too specific, but rather just the first symmetry allowed potential term. This approach is also in the spirit of the Lebwohl–Lasher [26] or Maier–Saupe family of potentials, which has proved extremely useful in modelling nematics. Such a very simplified model was actually introduced many years ago by Krieger and James (KJ) [27] for studying orientational transitions in solids. The model consists of a set of particles placed on a simple cubic lattice and interacting with the pair potential

$$U_{ij} = -\varepsilon_{ij}[P_2(\cos\beta_{ij}) + \xi P_1(\cos\beta_{ij})], \tag{1}$$

where ε_{ij} is a positive constant, ε, for nearest-neighbours particles i and j, β_{ij} is the angle between the axis of these two molecules and P_L is the Lth Legendre polynomial. In figure 1 we see this P_1P_2 potential for a few ξ values. In (1) the P_2 term plays the role of an aligning interaction, trying to bring the molecular axis parallel to one another, while the P_1 term represents a discriminating interaction that can distinguish the sense the second particle is placed with respect to the first. The parameter ξ determines the relative importance of the first-rank term with respect to the second one, while its sign determines ferroelectric or antiferroelectric type ordering or, in other words, if the particles prefer to align in the same sense or in the opposite one.

We should stress that use of the common terms ferroelectric or antiferroelectric does not imply that the discriminating force has to be an electric dipole. Indeed electric dipoles, if strong enough to provide a discrimination, would normally tend to pair out, corresponding to a negative ξ. Instead, it is worth pointing out that both signs of ξ can be of practical importance. For example we could have two situations

H–T	H–T
H–T	T–H
(a)	(b)

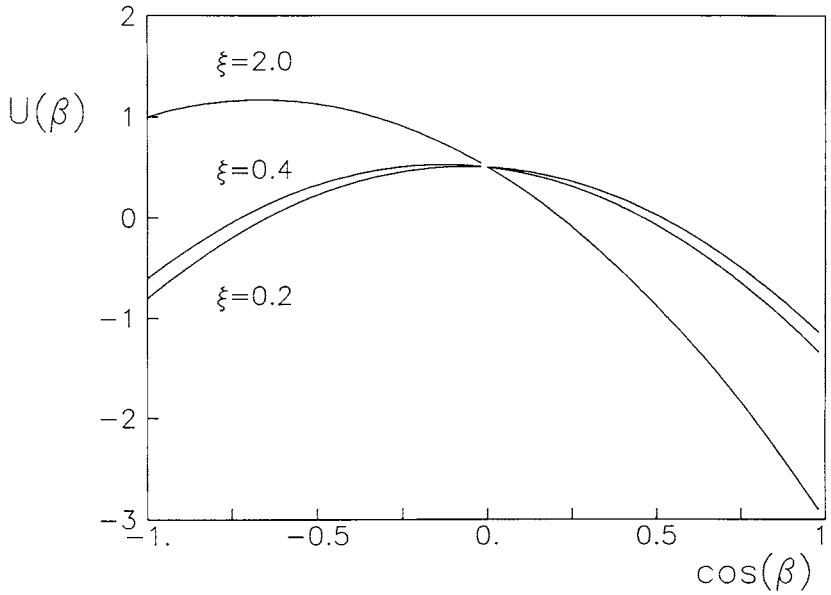

Figure 1. The angular dependence of the Krieger–James potential (1) for $\xi = 0{\cdot}2, 0{\cdot}4, 2{\cdot}0$.

where H is an aromatic fragment and T an alkyl chain, as mentioned before. Arrangement (a) would correspond to a pseudoferroelectric interaction, tending to bring heads and tails together with their likes. From a chemist's point of view, this arrangement can be quite reasonable and can actually be more common, because of the cumulative effect of the various intermolecular effects, than an antiferroelectric arrangement (b) that would be obtained for purely dipolar interactions. A pseudo ferroelectric arrangement is also likely when piling up bowl-shaped molecules [19–23], with H and T marking the upper, concave, part of the bowl and its bottom, respectively. The coefficients in (1) come from a general expansion of the potential and as such are not necessarily associated with a specific kind of intermolecular interaction. Rather they represent the sum of all the contributions to that rank from any kind of physical interaction.

In their pioneering study Krieger and James (KJ) obtained, using mean field theory (MFT) and, in some regions, an approximate cluster treatment, a phase diagram for this model. There it was found that there should exist various regions of the phase diagram corresponding to the ratio of first- to second-rank contributions. In particular at high ξ we should have a polar to isotropic transition and at low ξ both a polar and a non-polar (nematic-like) phase should exist. A triple point was found at $\xi = 0{\cdot}346$. This potential has also been used as a simple model for 'bowlic' liquid crystals by Lin Lei [19], who quoted in this different context the original phase diagram of KJ. It is worth noticing that going beyond molecular field theory is particularly important for a model like this. Indeed, MFT obtains the effective potential acting on a molecule by the combined effect of all the others. This effective potential then describes the change in energy of a molecule as its orientation referred to the director changes. The theory does not describe the ordering of one molecule with respect to the others and in particular of one molecule relative to its nearest neighbours. On the other hand it is clear that on a molecular level short range

ordering in this system will be important. We need to be able to distinguish between a situation where neighbouring molecules tend to be aligned in the same sense or in the opposite one. The model, with antiferroelectric interactions, has also been studied by Chandrasekhar and Madhusudana [10] again employing MFT and Bethe approximation, although in that case a phase diagram was not calculated and the aim was mainly on the effect of electric dipoles in the nematic phase. Other authors have used the model to gauge the influence of polar terms on the elastic constant in the nematic phase. Recently it has also been studied using Migdal transformation [28], although these results seem difficult to assess in view of the reported differences with computer simulation results obtained for other lattice models [28].

In this paper we shall go beyond mean field theory in two ways. First we present a detailed two-site cluster (TSC) study of the phase diagram. Secondly we describe Monte Carlo [29, 30] simulations for various values of ξ corresponding to different regions of the phase diagram. The simulations have the aim to check the two-site cluster (and of course molecular field) theory results and to get a general feeling for the goodness of the phase diagram they predict. This is particularly important here, where various transitions are predicted, since mean field theories are known to enhance the order of a transition [31]. Moreover, we wish to calculate for these selected situations some relevant observables, e.g. the pair distribution beyond nearest neighbours that none of the two previous methods can give.

2. Two-site cluster method

Two-site cluster theory treats in detail two particles in the field of all the others. The present method, already used by us [32] follows the lines of the classic work of Strieb, Callen and Horwitz [33, 34]. We start from the total energy

$$U_N = -\varepsilon \sum_{\langle i<j \rangle} \left(\sum_{L=1}^{2} \xi_L P_L(\cos \beta_{ij}) \right), \tag{2}$$

where $\xi_1 = \xi$ and $\xi_2 = 1$, the notation $\langle i < j \rangle$ indicates the different nearest-neighbour pairs of indices i, j. The key point of the cluster treatment is to approximate the Helmoltz free energy, A_N, as a sum of contributions from progressively larger clusters. This is obtained from suitable separation of U_N and in turn of the partition function

$$Z_N = \int \mathrm{d}\omega_1 \ldots \mathrm{d}\omega_N \exp\left(\frac{\varepsilon}{kT} \sum_{\langle i<j \rangle} \sum_{L=1}^{2} \xi_L P_L(\cos \beta_{ij}) \right), \tag{3}$$

where the molecular orientations are referred to the laboratory frame, chosen with the z axis along the potential director. The volume element is $\{\mathrm{d}\omega\} = \mathrm{d}\omega_1 \, \mathrm{d}\omega_2 \ldots \mathrm{d}\omega_N$, with $\mathrm{d}\omega_i = \mathrm{d}\alpha_i \sin \beta_i \, \mathrm{d}\beta_i$. We can consider the molecules arranged on two equivalent sublattices (this is true of simple cubic and body-centred cubic lattices), such that a molecule in one lattice has all its nearest neighbours in the other lattice and *vice versa*. Notice that there is a way, as pointed out by KJ, of mapping the ferroelectric into the antiferroelectric partition function and back. Let us assume that all the particles with odd indices are in a sublattice and the even labelled ones on the other sublattice. If one makes the coordinate transformation $\beta_j = \pi - \theta_j$ on all the particles belonging to one sublattice (e.g. j odd), this corresponds to arranging the molecules on a sublattice in an anti-parallel configuration with respect to the other ones. Since the partition is invariant for either choice of the coordinates, it follows that all thermal

properties derived from the orientational partition will be the same in both the cases. In other words an instantaneous configuration for the ferroelectric system gives, by changing by π all the β angles of the other sublattice, a configuration for the anti-ferroelectric system with the same energy. This does not mean that the average microscopic properties of the two systems will be equivalent or that they can be obtained one from the other. For instance, the configuration averaged odd-rank order paramters for the antiferroelectric system may be zero, while for the other they are quite different from zero. We shall see later on results for the order parameters and for the pair correlation function for two systems with opposite ξ. We rewrite the total energy as

$$U_N = -\varepsilon \sum_{\langle i<j \rangle} \sum_{L=1}^{2} \left(\xi_L \left[P_L(\cos\beta_i) P_L(\cos\beta_j) + \sum_{q \neq 0} D^L_{q0}(\omega_i) D^{L*}_{q0}(\omega_j) \right] \right), \quad (4)$$

using the spherical harmonics addition theorem [35]. Assuming that the lowest symmetry phase we can obtain is a C_∞ one, we need at most two variational parameters b_1, b_2 to separate the Hamiltonian in two parts: an unperturbed one,

$$U^0 = -\varepsilon \sum_{\langle i<j \rangle} \sum_{L=1}^{2} \xi_L \{ -b_L^2 + b_L [P_L(\cos\beta_i) + P_L(\cos\beta_j)] \}, \quad (5)$$

and in a perturbation U', non-linear in the expansion function

$$U' = -\varepsilon \sum_{\langle i<j \rangle} \sum_{L=1}^{2} \xi_L \{ P_L(\cos\beta_{ij}) + b_L^2 - b_L [P_L(\cos\beta_i) + P_L(\cos\beta_j)] \}. \quad (6)$$

The two parameters b_1 and b_2 introduced in this way are at this stage just arbitrary separation constants. Later we shall neglect some of the terms resulting from the separation and b_1, b_2 will be treated as adjustable variational parameters to be determined by requiring that the free energy is a minimum. As a consequence of the separation introduced in the potential, the free energy becomes a sum of two parts

$$A_N = A^0 + A', \quad (7)$$

where the unperturbed part,

$$\frac{-A^0}{kT} = -\frac{Nz\varepsilon}{2kT} \sum_{L=1}^{2} \xi_L b_L^2 + N \ln Z_1 - N \ln 2, \quad (8)$$

consists only of one particle contributions, with z the coordination number ($z = 6$ in our case) and Z_1 is a single particle pseudo-partition function,

$$Z_1 = \int_0^\pi d\beta \sin\beta \exp\left(\frac{z\varepsilon}{kT} \sum_{L=1}^{2} \xi_L b_L P_L(\cos\beta) \right). \quad (9)$$

At this level of approximation, the treatment is equivalent, after minimization of the free energy with respect to b_L,

$$\left(\frac{\partial A(b_1, b_2)}{\partial b_1} \right)_{b_2} = 0, \qquad \left(\frac{\partial A(b_1, b_2)}{\partial b_2} \right)_{b_1} = 0, \quad (10)$$

to molecular field theory and it would yield $b_L = \langle P_L \rangle$ for $L = 1,2$. An improvement over molecular field is obtained expanding the correction term $-A'$, following Strieb–Callen–Horwitz [33], in an infinite cluster series as

$$\frac{-A'}{kT} = -\sum_{\alpha=2} \frac{A'_\alpha}{kT}, \quad (11)$$

where the explicit general expression for the α cluster contribution is given in [33]. In practice we retain here the first correction term, obtaining the so-called two-site cluster approximation

$$\frac{-A'}{kT} \approx \frac{-A'_2}{kT} \tag{12a}$$

$$= \sum_{\langle i<j \rangle} \ln \left\langle \exp\left(\frac{-U'_{ij}}{kT}\right)\right\rangle_{U^0} \tag{12b}$$

$$= \tfrac{1}{2}Nz \ln Z_{12} - \frac{Nz\varepsilon}{2kT} \sum_{L=1}^{2} \xi_L b_L^2 - Nz \ln Z_1. \tag{12c}$$

The approximate free energy at two-site cluster level then becomes

$$\frac{-A_2}{kT} = \frac{-A^0 - A'_2}{kT} \tag{13a}$$

$$= \tfrac{1}{2}Nz \ln Z_{12} - (z-1)N \ln Z_1, \tag{13b}$$

where Z_{12} is the two particle pseudo-partition function,

$$Z_{12} = \int d\omega_1 \int d\omega_2 \exp\left(\frac{\varepsilon}{kT}\left[b_L(z-1)\sum_{L=1}^{2} \xi_L [P_L(\cos\beta_1) + P_L(\cos\beta_2)] + P_L(\cos\beta_{12})\right]\right). \tag{14}$$

The condition of minimum free energy with respect to the parameters b_L gives the two consistency conditions

$$\langle P_L \rangle_{Z_1} = \tfrac{1}{2}\langle P_L(\cos\beta_1) + P_L(\cos\beta_2)\rangle_{Z_{12}}, \qquad L = 1, 2, \tag{15}$$

where we indicate with $\langle \ldots \rangle_{Z_1}$, $\langle \ldots \rangle_{Z_{12}}$ the averages performed with the one- and two-particle distributions (cf. (9), (14)). In practice we shall refer the free energy to the standard isotropic state with complete disorder, thus we shall subtract the infinite temperature contribution.

The various thermodynamic observables are obtained from the free energy. The energy is obtained differentiating the free energy with respect to $\beta_T \equiv 1/kT$ and inserting the self-consistency conditions. This gives

$$\langle U_N \rangle = -\frac{Nz\varepsilon}{2}(\xi\sigma_1 + \sigma_2), \tag{16}$$

where σ_1, σ_2 are short-range order parameters

$$\sigma_L = \langle P_L(\cos\beta_{12})\rangle_{Z_{12}}, \tag{17}$$

equal to the value of the rotationally invariant pair correlation at nearest-neighbour distance $r = a$ [30]

$$\sigma_L = G_L(a). \tag{18}$$

As already mentioned the ability to calculate short-range order parameters represents an important advantage of two-site cluster over mean field theory. There in fact the relative order of two particles is the same for arbitrary separations and $\sigma_L = \langle P_L \rangle^2$. In particular no short-range nematic order is predicted in the isotropic phase and no residual short-range polar order is predicted by mean field theory in the nematic phase.

An expression for the TSC heat capacity $C_V^* \equiv C_V/kN$ is obtained differentiating the energy with respect to temperature

$$C_V^* = -\beta_T^2 \left(\frac{\partial U}{\partial \beta_T}\right)_V \tag{19a}$$

$$= \frac{z\varepsilon^2}{2(kT)^2} \sum_{L=1}^{2} \xi_L \left(\frac{\partial \sigma_L}{\partial \beta_T}\right)_V. \tag{19b}$$

An analytic equation for the heat capacity can be obtained by first differentiating σ_2 in (17) with respect to β_T. This gives an expression in terms of the temperature derivatives of the variational parameters $\partial b_L/\partial \beta_T$. This in turn can be obtained by solving the linear system obtained differentiating both sides of (15) with respect to β_T and solving the resulting two by two system. We do not report the resulting equation, since it is too complicated, although it is available to interested readers. The heat capacity results obtained in this way have been satisfactorily checked with the simpler process of direct numerical differentiation of the energy.

2.1. *Details of the two-site cluster calculations*

We have obtained the two-site cluster variational parameters b_1 and b_2 by direct numerical minimization of the free energy, rather than by solving the system of consistency equations. In practice we have used the MINUIT non-linear minimization package from CERN [36] performing first a Monte Carlo search, then a refinement of the minimum found using a gradient method. We have verified that the consistency conditions are satisfied at the minimum. Working with double precision in VAX FORTRAN we obtained the sum of residuals Δ,

$$\Delta = \left(\sum_{L=1}^{2} |\langle P_L \rangle - \tfrac{1}{2}\langle P_L(\cos\beta_1) + P_L(\cos\beta_2)\rangle|^2 \right)^{1/2} \tag{20}$$

always lower than 10^{-6}. Minimization at a temperature near a previously studied one was started from the variational parameters obtained before. In our opinion direct minimization of the free energy functional presents several advantages, especially when various potential thermodynamic phases exist. First the free energy functional is concave in the parameters space, with an absolute minimum corresponding to the equilibrium solution. On the contrary, solution of the consistency equations (15) can give unstable or plainly non-physical solutions as well as the stable ones. Direct minimization also requires a smaller number of integrals to be evaluated. For the present case it requires calculating Z_1, Z_{12}, while the consistency equations require six, i.e. Z_1, Z_{12}, $\langle P_1\rangle_{Z_1}$, $\langle P_2\rangle_{Z_1}$, $\langle P_1\rangle_{Z_{12}}$, $\langle P_2\rangle_{Z_{12}}$. The calculation of this set of integrals has of course to be repeated at every step of an iterative procedure and the saving in computer time can be substantial, especially for problems depending on more than one variable.

3. Computer simulations

3.1. *Cluster Monte Carlo*

Our aim here is to determine the phase transitions of the KJ system for a set of ξ values in order to determine the corresponding points in the phase diagram. Determining transition temperatures and transition behaviour is a challenging exercise in computer simulations [37]. To this end the choice of boundary conditions, i.e. of

what environment to surround the sample with, is very important. The standard method is to use periodic boundary conditions (PBMC) and consists of having replicas of the sample box filling up as much space as needed by the range of the pair interaction. Although clearly superior to a free space boundary, using periodic boundary conditions leads to large smearing and broadening of the heat capacity and order parameter derivative versus temperature peaks at a supposed transition. This complicates the location of the transition itself and in turn often means that relatively large samples, with many thousands of particles may have to be used [37]. Thus we have first simulated the P_1P_2 system employing the Cluster Monte Carlo (CMC) method. In this technique, described in detail in [38], periodic boundary conditions are replaced by a weaker condition that the particles inside and outside the sample box have, on the mean, the same observable properties of those inside, rather than being their exact replicas. The desired bulk average of a quantity A is written as an average over the external 'world' configurations [W] of the average values $\langle A\rangle_{[W]}$ calculated for a fixed configuration of the 'world' outide the sample box. In practice a finite set M_W of external world configuration samplings is used and one has that a single Monte Carlo average is replaced by an average of Monte Carlo results obtained for a fixed environment [W]

$$\langle A\rangle \approx \frac{1}{M_W}\sum_{[W]}\langle A\rangle_{[W]}. \tag{21}$$

In practice the outside world configurations needed are obtained by creating a zone of ghost particles outside the sample box having on average the same ordering properties and, in particlar, the same singlet distribution and order parameters of the system inside the box. Thus we assume a symmetry breaking field direction, defining the Z laboratory axis and that the ordered phase is at most uniaxial around this direction. We then calculate the order parameters relative to this direction, which for the present case are just the Legendre polynomial averages $\langle P_L\rangle_{LAB}$, i.e. $\langle P_1\rangle_{LAB}$, $\langle P_2\rangle_{LAB}, \ldots, \langle P_{L'}\rangle_{LAB}$,

$$\langle P_L\rangle_{LAB} = \frac{1}{N}\sum_i^N P_L(\cos\beta_i). \tag{22}$$

We proceed constructing the best Information Theory [39] inference for the orientational distribution of the particles outside the sample based on these observables,

$$P(\cos\beta) = \exp\left(\sum_{L=0}^{L'} a_L P_L(\cos\beta)\right), \tag{23}$$

where the coefficients a_L are determined from the constraint that the available $\langle P_L\rangle$ can be reobtained by averaging $P_L(x)$ over the distribution, with a_0 determined by the normalization condition. In most cases studied we have used the first two relevant order parameters, $\langle P_1\rangle$ and $\langle P_2\rangle$, so that the most likely distribution has been taken of the form

$$P(\cos\beta) = \frac{\exp[a_1P_1(\cos\beta) + a_2P_2(\cos\beta)]}{\int_0^\pi d\beta \sin\beta \exp[a_1P_1(\cos\beta) + a_2P_2(\cos\beta)]}. \tag{24}$$

The coefficients a_1, a_2 are in turn determined by solving the non-linear system

$$\langle P_1\rangle_{\mathrm{LAB}} = \frac{\int_0^\pi \mathrm{d}\beta \sin\beta\, P_1(\cos\beta) \exp\left[a_1 P_1(\cos\beta) + a_2 P_2(\cos\beta)\right]}{\int_0^\pi \mathrm{d}\beta \sin\beta \exp\left[a_1 P_1(\cos\beta) + a_2 P_2(\cos\beta)\right]}, \tag{25a}$$

$$\langle P_2\rangle_{\mathrm{LAB}} = \frac{\int_0^\pi \mathrm{d}\beta \sin\beta\, P_2(\cos\beta) \exp\left[a_1 P_1(\cos\beta) + a_2 P_2(\cos\beta)\right]}{\int_0^\pi \mathrm{d}\beta \sin\beta \exp\left[a_1 P_1(\cos\beta) + a_2 P_2(\cos\beta)\right]}. \tag{25b}$$

In two simulations we have generated the distribution outside the sample using order parameters up to $L' = 3$ in (23) and accordingly we have solved a system of three nonlinear equations. The numerical solution of this system is performed using IMSL library routines [32, 40]. The results we obtain are shown in figure 2. Notice that the coefficients $a_1(\langle P_1\rangle, \langle P_2\rangle)$ and $a_2(\langle P_1\rangle, \langle P_2\rangle)$ are not defined in the entire $(\langle P_1\rangle, \langle P_2\rangle)$ plane, but in a domain delimited by the inequalities

$$\tfrac{2}{3}\langle P_2\rangle + \tfrac{1}{3} \leqslant \langle P_1\rangle \leqslant (\tfrac{2}{3}\langle P_2\rangle + \tfrac{1}{3})^{1/2}. \tag{26}$$

These restrictions follow in turn from Schwarz's inequality [41] applied to the specific trigonometric form of the first- and second-rank Legendre polynomials. The inversion of $\langle P_1\rangle$, $\langle P_2\rangle$ to give a_1, a_2 gets numerically difficult and has to be performed with some care at high order, since an asymptotically large value of the parameters would need to be obtained as the orientational order parameters are in reach of their boundary value of one.

We have studied three systems of particles interacting with the $P_1 P_2$ potential (1) on a simple cubic lattice with dimensions $8 \times 8 \times 8$ for values of the first-rank to second-rank ratio $\xi = 0{\cdot}2$, $\xi = 0{\cdot}4$, $\xi = 2{\cdot}0$. We have also simulated $10 \times 10 \times 10$ lattices for $\xi = -0{\cdot}2$, $\xi = 0{\cdot}14$, $\xi = 0{\cdot}3$. The calculations have been run in cascade in a heating sequence. The first was started from a completely aligned system at low temperatures and the others were normally initiated from an already equilibrated configuration at the nearest lower temperature. The CMC procedure has then been followed, thus, Metropolis Monte Carlo procedure has been used to update the lattice for a certain number of cycles, i.e. of sets of N attempted moves. Each particle is selected at random for an attempted move at every lattice sweep with a shuffling algorithm [37] and a new trial orientation of the chosen particle is then generated by a controlled deviation from the previous one [42]. We have checked that an acceptance ratio not too far from 0·5 is achieved in this way. After a pre-equilibration period the order parameters $\langle P_1\rangle_{\mathrm{LAB}}$ and $\langle P_2\rangle_{\mathrm{LAB}}$ inside the sample are calculated. These two parameters are used to determine a_1 and a_2 and thus the distribution in (24) from which new orientations for the ghost particles outside the box are sampled. For the $\xi = 0{\cdot}14$ and $\xi = 0{\cdot}2$ simulations, $\langle P_3\rangle$ has also been used. We generate the orientations of these external ghost molecules utilizing a simple rejection technique [14] and check that both the order parameters $\langle P_1\rangle_{\mathrm{out}}$ and $\langle P_2\rangle_{\mathrm{out}}$ relative to the particles outside are the same as those inside calculated over M_k cycles to an acceptable threshold θ_1, θ_2 defined as 0·05 statistical confidence level [43] as follows

$$\theta_L = 1{\cdot}96[v^2(\langle P_L\rangle_{\mathrm{out}}) + v^2(\langle P_L\rangle_{\mathrm{in}})]^{1/2} \qquad L = 1, 2, \tag{27}$$

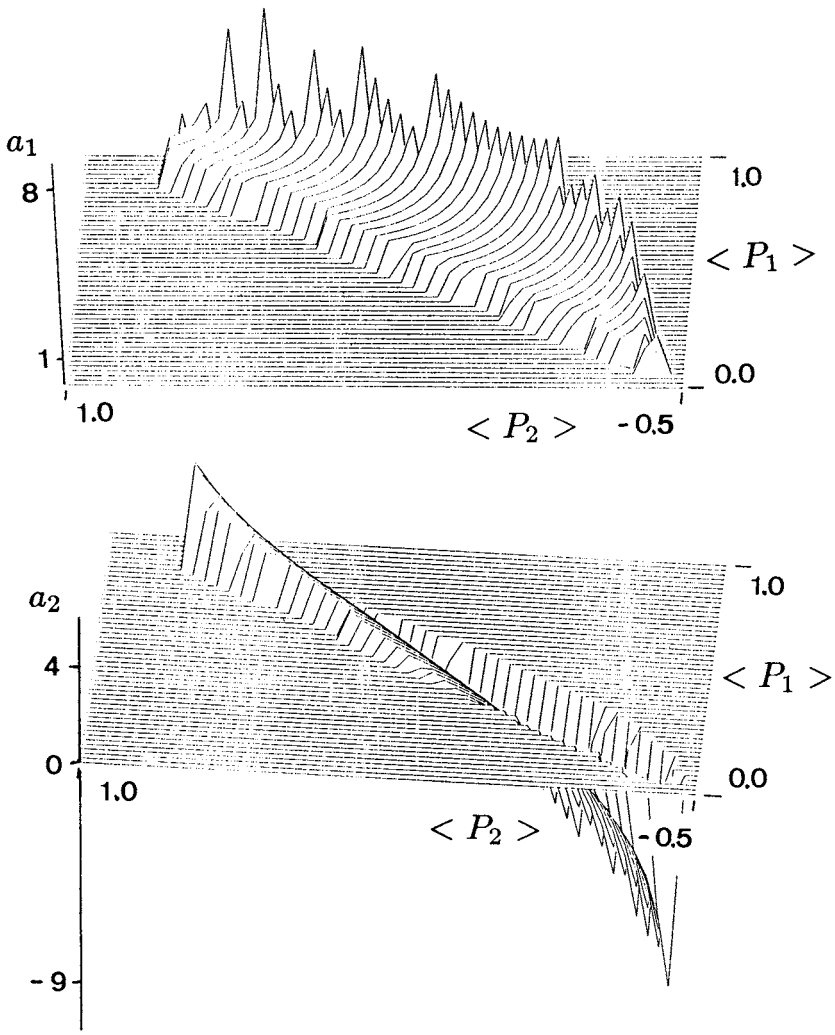

Figure 2. The maximum entropy coefficients (a) a_1, (b) a_2 defining the distribution in (24) as a function of the order parameters $\langle P_1 \rangle$ and $\langle P_2 \rangle$.

where $v(\langle P_L \rangle)$ is the variance. The generation is repeated if

$$|\langle P_L \rangle_{\text{out}} - \langle P_L \rangle_{\text{in}}| \geqslant \sigma_g,$$

i.e., if the order parameters inside and outside the sample differ for more than a threshold value σ_g. The energy of the system is then recalculated and evolution proceeds as before. A small number (10–20) of micro re-equilibration sweeps is discarded, then the new MC trajectory is followed in the usual way. In all the subsequent cycles the order parameters with respect to the Z laboratory direction P_L^J for the molecules inside the box are still calculated. After a certain number of cycles M_K an average is calculated for this K trajectory segment together with the attendant standard deviation v_K. These internal order parameters are then compared to the ones outside. If the difference between them is statistically significant to a satisfactory

confidence level [43] σ_1,

$$\sigma_1 = 1{\cdot}96\left(\frac{v_K^2(\langle P_L\rangle)}{M_K} + \frac{v_{K-1}^2(\langle P_L\rangle)}{M_{K-1}}\right)^{1/2}, \tag{28}$$

a new set of orientations for the ghost molecules is generated using the new order parameters. If the order parameters inside and outside are not significantly different the orientations outside are kept and the next check is made after a longer segment, i.e. $M_{K+1} > M_K$. The number of cycles M_K is instead left constant if the order was adjusted. This ensures on one hand that we do not choose incorrect order parmeters outside and leave them unchanged. On the other hand since every change of the outside layer will lower the short range correlation at the interface this method takes care to do the updating only if really needed and not on every cycle or on the basis of some wild fluctuation. A number of observables are calculated, as we shall see in detail later on.

3.2. *Periodic boundary conditions Monte Carlo*

We have studied a system of $N = 1000$ particles employing the standard Monte Carlo Metropolis method with periodic boundary conditions (see, e.g. [30]) to get a comparison with the CMC method. We have chosen a value of $\xi = 0{\cdot}2$ where both a polar and a nematic phase is predicted to exist. The simulation has been run in a completely independent manner from the previous CMC ones, so once more the run at the lowest temperature studied has been initiated from a completely aligned system. The calculations at the other temperatures have been started in cascade from an equilibrium configuration at the nearest lower temperature. The same controlled configuration updating procedure mentioned in the previous section [42] has been employed.

3.3. *Details of the simulation*

Every property of interest, A, is evaluated at every cycle. After a certain number of cycles m_J (here 2000) an average A^J is calculated thus providing an effective coarse graining of the trajectory. A further grand average is then computed as the weighted average over M such supposedly uncorrelated segments. The attendant weighted standard deviation from the average σ_A is also calculated and gives the error estimates shown in the figures. We have calculated for each simulation energy, first-$\langle P_1\rangle_\lambda$, second-$\langle P_2\rangle_\lambda$ and fourth-$\langle P_4\rangle_\lambda$ rank order parameters. $\langle P_2\rangle_\lambda$ has been evaluated as the largest eigenvalue of the ordering matrix as described in [30]. A first-order parameter (the instantaneous polarization) is calculated as follows. We recall that the eigenvector corresponding to the largest eigenvalue of the ordering matrix yields the location of the instantaneous director $\boldsymbol{d}^J$. We then compute an average P_1 from the scalar product between the director and the unit vectors $\boldsymbol{u}_i$ specifying each particle orientation in the laboratory frame. This sample averaged quantity for the Jth configuration

$$\langle P_1\rangle_\lambda^J = \frac{1}{N}\left|\sum_i^N \boldsymbol{u}_i \cdot \boldsymbol{d}^J\right| \tag{29}$$

is further averaged over M configurations to give the polarization $\langle P_1\rangle_\lambda$ as

$$\langle P_1\rangle_\lambda = \frac{1}{M}\sum_J^M \langle P_1\rangle_\lambda^J. \tag{30}$$

Fourth-rank order parameters have been computed with the algorithm introduced in [37]. These order parameters give the ordering with respect to the instantaneous director. For the CMC method [38], where an external laboratory direction exist, order parameters $\langle P_L \rangle$ with respect to the director have also been calculated. Pair correlation coefficients [30] again of second and fourth rank have been calculated at selected temperatures as described in [30, 37].

4. Results and discussion

Here we present the results of simulations and compare them with the two-site cluster findings. We start with the phase diagram obtained from two-site cluster theory, shown as the continuous lines in figure 3. This was obtained running a total of 52 different ξ cases. For each of these a detailed temperature scan was performed, refining near the transitions. The character of a phase change and its properties were estimated by running a heating and a cooling sequence across the transition with temperature steps of the order of 10^{-5} reduced units. In this way it was found possible to follow the high and low temperature phase free energy with their metastable branches and their intersection. The transition temperatures were then confirmed by further refining until a free energy difference between the two adjacent phases below 10^{-6} was attained. We estimate our transition temperatures to be accurate to the fourth figure, even though we shall just quote TSC results rounded to the third, because of the approximations built into the procedure itself. As we see from figure 3 the phase diagram is in qualitative agreement with that of Krieger and James [27]. We also find three phases: polar, nematic and isotropic and a similar overall shape for the phase diagram. In particular at low polar contributions a polar to nematic to isotropic sequence is found. On the contrary at high ξ the system goes directly from polar to isotropic. However, there are significant quantitative differences. The three phases coexist at a triple point

$$\xi_T = 0{\cdot}3578, \quad \text{with} \quad T^* = 1{\cdot}2202,$$

where we introduce the dimensionless temperature $T^* \equiv kT/\varepsilon$. The triple point was located by KJ at

$$\xi_T^{KJ} = 0{\cdot}346, \quad \text{with} \quad (T^{KJ})^* = 1{\cdot}3212.$$

Krieger and James divided the phase diagram in five regions of ξ (shaded in figure 3). The character of the transition varies in these regions, as we see from figure 4 where we plot the latent heat ΔU^*. Even though the precise location of the different regions indicated by the shadings cannot always be appreciated on a diagram like this, it is apparent that the polar transition changes from a second-order to a first-order one with $1/\xi$, while the nematic–isotropic transition is always characterized by a finite heat of transition. We compare here our results with those of Krieger and James (in brackets).

Range I $0 < 1/\xi < 0{\cdot}61(0{\cdot}6)$
This is a situation dominated by the discriminating interaction. The system has a polar phase, characterized by non vanishing $\langle P_1 \rangle$ and $\langle P_2 \rangle$ and becomes isotropic with a second-order polar–isotropic transition.

Range II $0{\cdot}61(0{\cdot}6) \leqslant 1/\xi < 1{\cdot}82(1{\cdot}7)$
Here we still have only a polar ordered phase, however, the polar to

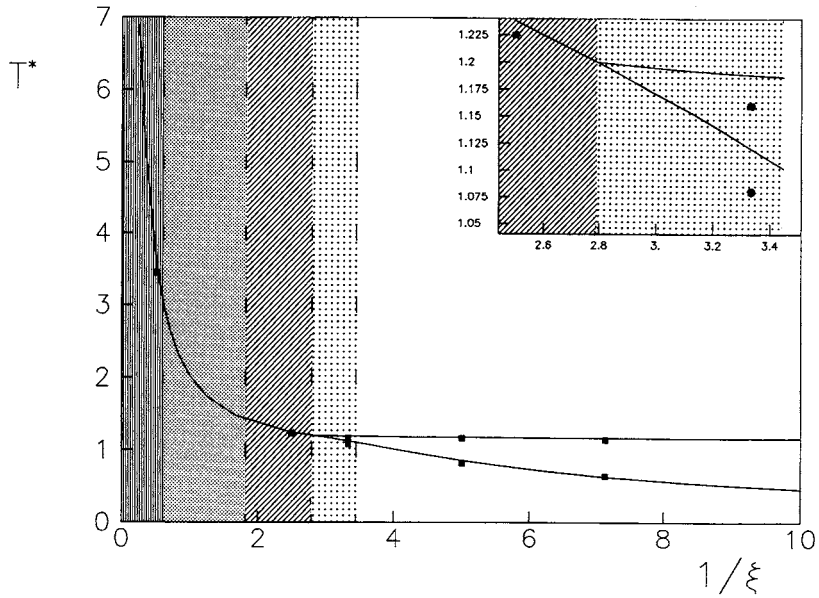

Figure 3. The phase diagram determined by two-site cluster theory (continuous line) and Cluster Monte Carlo results $\xi = 0{\cdot}14, 0{\cdot}2, 0{\cdot}3, 0{\cdot}4, 2{\cdot}0$ (■). $T^* \equiv kT/\varepsilon$ is the dimensionless temperature. The inset shows a close up of the triple point region, $\xi \geqslant 0{\cdot}3578$, $T^* = 1{\cdot}200\,22$. The different shaded areas correspond to regions where the character of the transitions changes (cf. text and next figure).

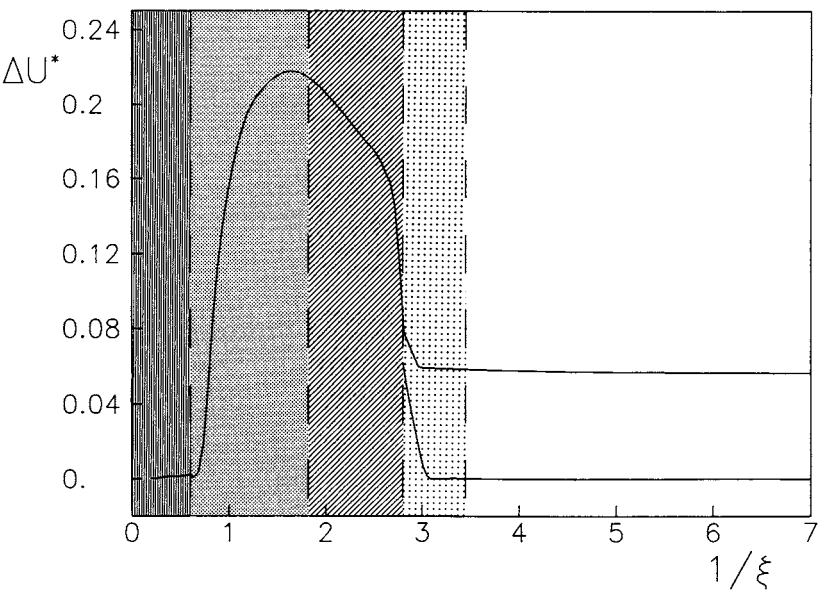

Figure 4. The latent heat of transition as obtained from two-site cluster theory reported as a function of the inverse polar contribution term $1/\xi$. The shaded areas correspond to the ranges where the transition from the polar phase changes character. Of the two curves starting in the dotted area the top one refers to the nematic–isotropic transition, the other to the polar to nematic one.

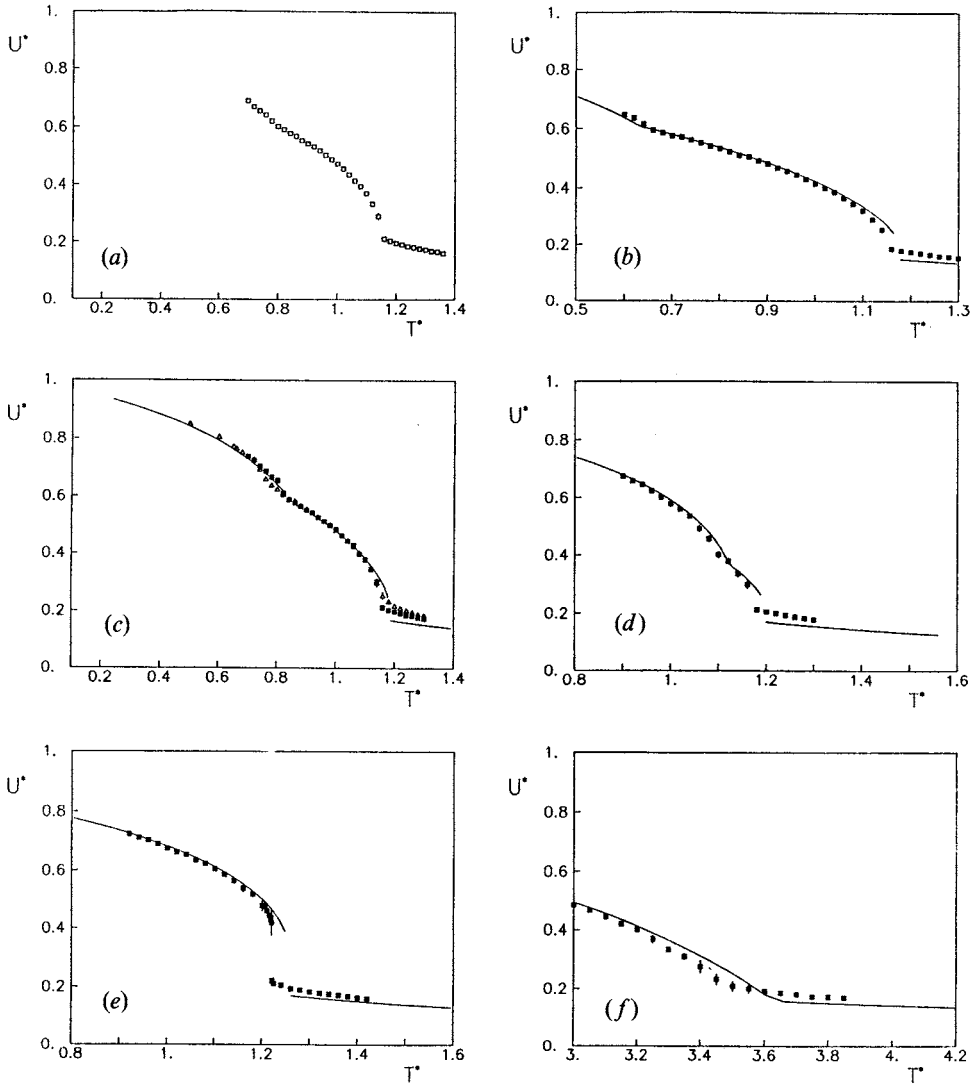

Figure 5. The single particle energy, $U^* = \langle U \rangle / N\varepsilon$, as a function of the dimensionless temperature $T^* = kT/\varepsilon$ for the model with ξ (*a*) −0·2, (*b*) 0·14, (*c*) 0·2, (*d*) 0·3, (*e*) 0·4 and (*f*) 2·0. The results are for Cluster Monte Carlo simulations (■, □) for periodic boundary conditions Monte Carlo simulation (△), and two-site cluster theory (——).

isotropic transition is now first order, as we can see from the latent heat in figure 4.

Range III $1{\cdot}82(1{\cdot}7) \leqslant 1/\xi < 2{\cdot}7949(2{\cdot}890)$
Here we have a first-order polar to isotropic transition and a metastable nematic.

Range IV $2{\cdot}7949(2{\cdot}890) < 1/\xi \leqslant 3{\cdot}45(3{\cdot}2103)$
For this ξ span we have not only the polar phase but also a nematic, with $\langle P_1 \rangle = 0$ and $\langle P_2 \rangle \neq 0$. Both the polar–nematic and the nematic to isotropic transition are of first order.

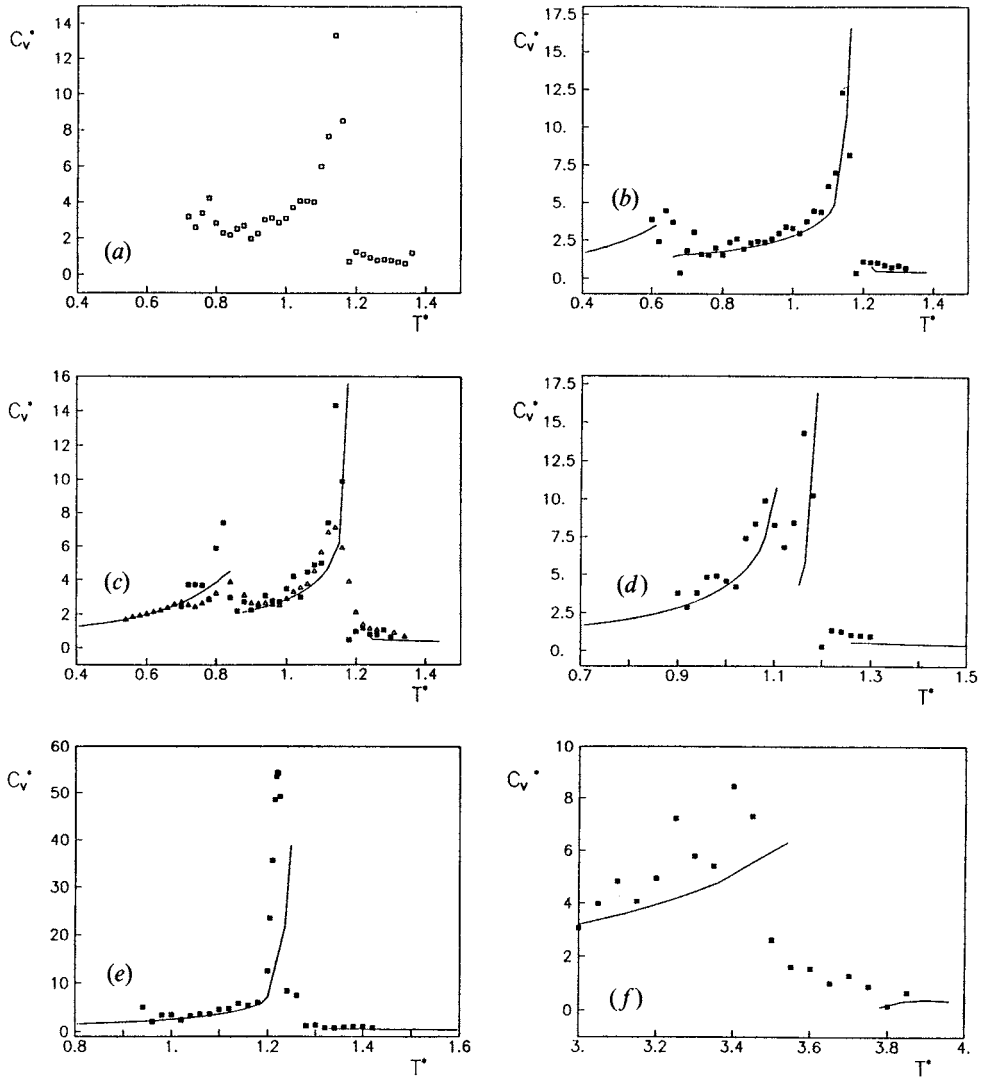

Figure 6. The heat capacity, C_V^* against dimensionless temperature $T^* = kT/\varepsilon$ for the model with ξ (*a*) −0·2, (*b*) 0·14, (*c*) 0·2, (*d*) 0·3, (*e*) 0·4 and (*f*) 2·0. The results are for Cluster Monte Carlo simulations (■, □), for periodic boundary conditions Monte Carlo simulation (△), and two-site cluster theory (——).

Range V $1/\xi > 3{\cdot}45(3{\cdot}2103)$
This is the region of smallest discriminating contributions. We still have two phases, but the polar to nematic transition is second order, while the nematic–isotropic is first order.

Since we have adopted an algorithm, based on direct minimization of the free energy, different from the usual solution of consistency conditions, we have verified that KJ results can be recovered by truncating the cluster series at the first term (mean field theory level). The difference is thus to be assigned not to the different way of solving the problem but to the usual overestimation of the transition presented by

Table 1. The nematic–isotropic transition temperatures $(T^*_{NI})_{C_v}$ for the KJ model with $\xi = -0{\cdot}2, 0{\cdot}14, 0{\cdot}2, 0{\cdot}3$ as obtained from the PBMC and CMC computer simulations and from TSC theory. We also report the estimates for the transition values of the heat capacity, the first-rank $\langle P_1 \rangle$ and the second-rank order parameter $\langle P_2 \rangle$ obtained, in the case of simulations, from the diagonalization procedure. The nematic–isotropic transition remains first order and the order at the transition remains essentially constant at different ξ.

ξ	Method	$(T^*_{NI})_{C_v}$	$(C^*_{max})_{NI}$	$\langle P_1 \rangle_{NI}$	$\langle P_2 \rangle_{NI}$
$-0{\cdot}2$	CMC	1·14	13·4 ± 0·5	0·015 ± 0·01	0·37 ± 0·03
0·14	CMC	1·14	12·3 ± 0·5	0·03 ± 0·01	0·36 ± 0·02
	TSC	1·166	16·6	0·0	0·387
0·2	PBMC	1·14	7·1 ± 0·5	0·03 ± 0·01	0·34 ± 0·02
	CMC	1·14	14·3 ± 0·9	0·04 ± 0·01	0·40 ± 0·02
	TSC	1·173	15·6	0·0	0·387
0·3	CMC	1·16	14·3 ± 0·8	0·05 ± 0·01	0·39 ± 0·03
	TSC	1·188	16·9	0·0	0·387

their mean field theory [37]. We notice that the polar interactions are in general stabilizing an orientationally ordered phase compared to the isotropic one. Indeed we see by looking at the phase diagram that the transition moves to higher temperatures as ξ increases. This is true also for small ξ and is to be expected from thermodynamic perturbation theory [44]. Indeed if we consider the purely second-rank potential as a reference, a first-rank perturbation has a different symmetry and does not contribute at first order to the energy. The non-vanishing second-rank contribution always has a negative sign and leads to energy stabilization.

The Cluster Monte Carlo phase diagram results are also reported in figure 3 as the square symbols and as we see they confirm the two-site cluster findings. As mentioned before we studied three $8 \times 8 \times 8$ ($\xi = 0{\cdot}2, 0{\cdot}4, 2{\cdot}0$) and three $10 \times 10 \times 10$ ($\xi = -0{\cdot}2, 0{\cdot}14, 0{\cdot}3$) systems with CMC method and a $10 \times 10 \times 10$ ($\xi = 0{\cdot}2$) with the PBMC method. For each of these systems a large number of temperature

Table 2. The polar–nematic transition temperature $(T^*_{PN})_{C_v}$ for the KJ model with $\xi = -0{\cdot}2$, $0{\cdot}14, 0{\cdot}2, 0{\cdot}3$ as obtained from the PBMC and CMC computer simulations and from TSC theory. We also report the estimates for the transition values of the heat capacity, the first rank ($\langle P_1 \rangle$) and the second-rank ($\langle P_2 \rangle$) order parameter as obtained from PBMC, CMC simulations and using TSC theory. The transition is a steep continuous one for $\xi = -0{\cdot}2, 0{\cdot}14, 0{\cdot}2$ so we report the values of the order parameters at the point immediately after the transition. We cannot assign the character of the transition at $\xi = 0{\cdot}3$ (this is in range IV).

ξ	Method	$(T^*_{PN})_{C_v}$	$(C^*_{max})_{PN}$	$\langle P_1 \rangle_{PN}$	$\langle P_2 \rangle_{PN}$
$-0{\cdot}2$	CMC	0·78	4·2 ± 0·8	0·015 ± 0·001	0·782 ± 0·002
0·14	CMC	0·64	4·5 ± 0·5	0·03 ± 0·02	0·82 ± 0·01
	TSC	0·632	3·5	0·0005	0·843
0·2	PBMC	0·84	3·9 ± 0·5	0·05	0·747 ± 0·001
	CMC	0·84	7·4 ± 0·5	0·06 ± 0·01	0·767 ± 0·01
	TSC	0·8562	4·5	0·020	0·7614
0·3	CMC	1·08	9·9 ± 0·5	–	0·61 ± 0·01
	TSC	1·116	10·9	0·2016	0·5763

Table 3. The polar–isotropic transition temperature $(T^*_{PI})_{C_v}$ and properties, as in table 1. The transition for $\xi = 0{\cdot}4$ (belonging to range III in the phase diagram) is a first-order one and the values reported are just before the jump to isotropic. On the contrary the transition for $\xi = 2$ is a broad continuous one (cf. figures 7 and 8) and the first and second rank order parameters given are just those at the temperature corresponding to the heat capacity peak.

ξ	Method	$(T^*_{PI})_{C_v}$	$(C^*_{max})_{PI}$	$\langle P_1 \rangle_{PI}$	$\langle P_2 \rangle_{PI}$
0·4	CMC	1·22	54 ± 10	0·54 ± 0·09	0·52 ± 0·04
	TSC	1·238	38·8	0·575	0·552
2·0	CMC	3·40	8·5 ± 0·9	0·38 ± 0·08	0·13 ± 0·03
	TSC	3·625	6·9	0·0452	0·0015

runs were performed, as we can see from the figures, where the results of a total of about 200 runs are collected together. To start with we show in figure 5 the energy as a function of temperature. The temperature range is normally different for the various systems to concentrate on the respective transition regions. Notice, however, the comparison between the system with $\xi = -0{\cdot}2$ (top left) and $\xi = 0{\cdot}2$ (just below that) which shows that the behaviour for the two systems is essentially the same. This is to be expected for the argument reported in section 2 [27], even though here we are talking of actual computer experimental results on finite systems.

The heat capacity obtained by simulation and by TSC is shown in figure 6. It is obtained by performing a quasi-cubic Hermite interpolation [40] of the energy against temperature points and differentiating. The transition temperatures for the simulations were located from the heat capacity and the order parameter derivative peaks.

Our estimates for the transition temperatures and properties are given in tables 1 to 3 for the nematic–isotropic, polar–nematic and polar–isotropic transitions, respectively. As we have already seen both Krieger and James and two-site cluster calculations have found that the character of the polar to isotropic transition changes from first- to second-order as the strength of the polar contribution, ξ, increases moving away from the triple point. The polar to nematic transition also changes character, being second order for very small ξ. We could not examine all of these features of the phase diagram with computer simulation at least at this stage. The change in character of the transitions with ξ is, however, apparent from the energies and heat capacities.

In the transition regions the simulations presented some difficulties of convergence and fairly long runs were required. For the PBMC simulation we have used at least 15 000 equilibration cycles far from the transition and 25 000 in the pseudocritical region. For the CMC simulations we have in general discarded at least 20 000 and 30 000 equilibration cycles before starting production respectively when far or near the transition. At low ξ values (0·14, 0·2) and at low temperature equilibration was extremely slow. We have discarded up to 3×10^5 cycles in these few cases. The production runs were also of varying length, according to the distance from the transition. Close to a phase change sequences of about 4 kcycles have been used for the CMC and for the PBMC simulation.

The increase of the proportion of discriminating interaction has quite a profound effect on the behaviour of the system. For $\xi = 0{\cdot}14$ and 0·2 the system undergoes two transitions. The separation in temperature between the two transitions decreases as ξ increases. For $\xi = 0{\cdot}3$ the two transtions are very near (cf. inset in figure 3). For the two higher values of ξ only one transition is apparent. A plot of the first-rank

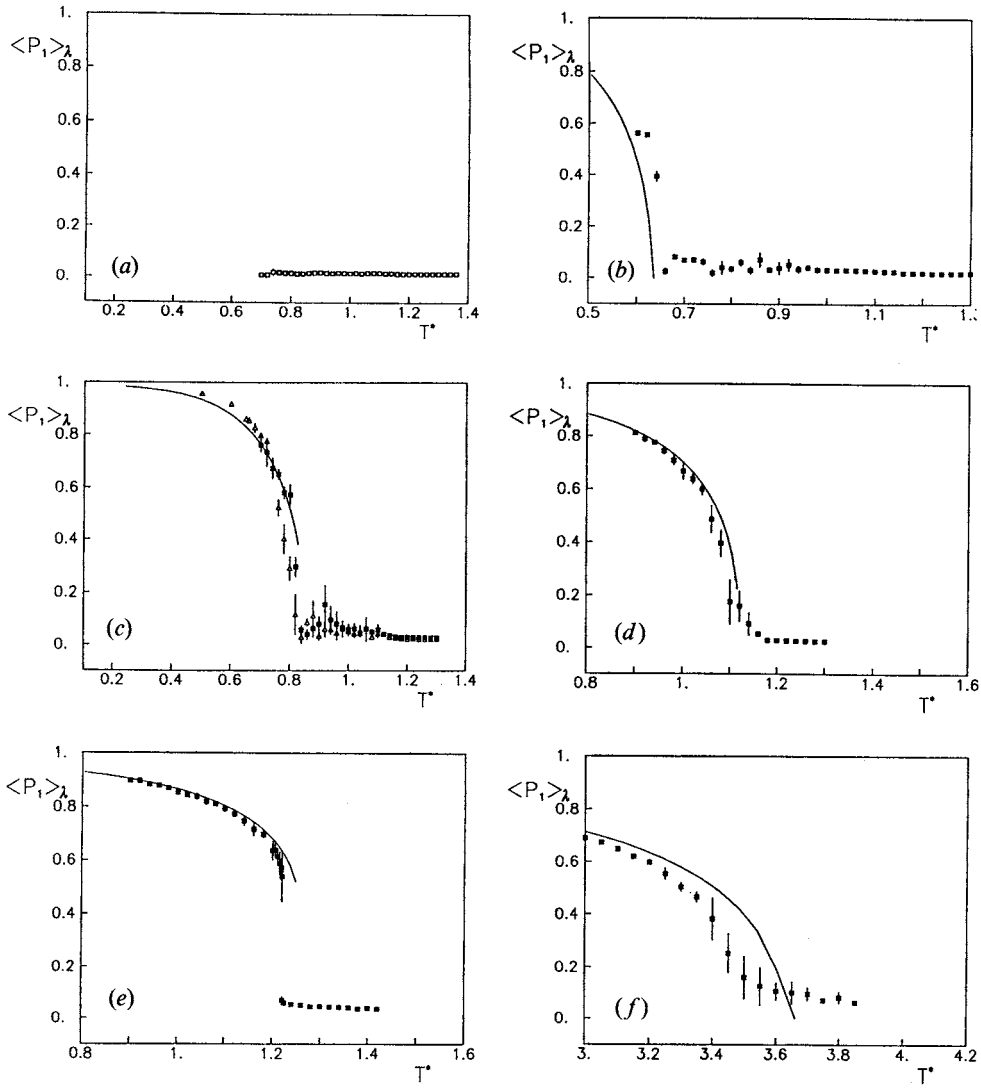

Figure 7. The first-rank order parameter $\langle P_1 \rangle$ plotted against reduced temperature T^* obtained from CMC (■, □) at ξ (*c*) 0·2, (*e*) 0·4, (*f*) 2·0 (8 × 8 × 8 lattice) and ξ (*a*) −0·2, (*b*) 0·14, (*d*) 0·3 (10 × 10 × 10 lattice), from 10 × 10 × 10 PBMC (△) (only ξ = 0·2), and TSC theory (——). Notice the different temperature ranges for the various cases.

order parameter against temperature as shown in figure 7 manifests that the low temperature phase is a polar one with $\langle P_1 \rangle \neq 0$.

Above the first transition, if present, $\langle P_1 \rangle$ is zero within our experimental error. A similar plot for the second-rank order parameter, shown in figure 8, demonstrates that $\langle P_2 \rangle$ is greater than zero between the first and second transition and in general up to the highest temperature change of phase. The order parameters $\langle P_L \rangle_{LAB}$ have similar behaviour and are not reported, thus we can call by metaphor this mesophase a nematic one. Noticed that the occurrence of the polar to nematic transition goes unnoticed if

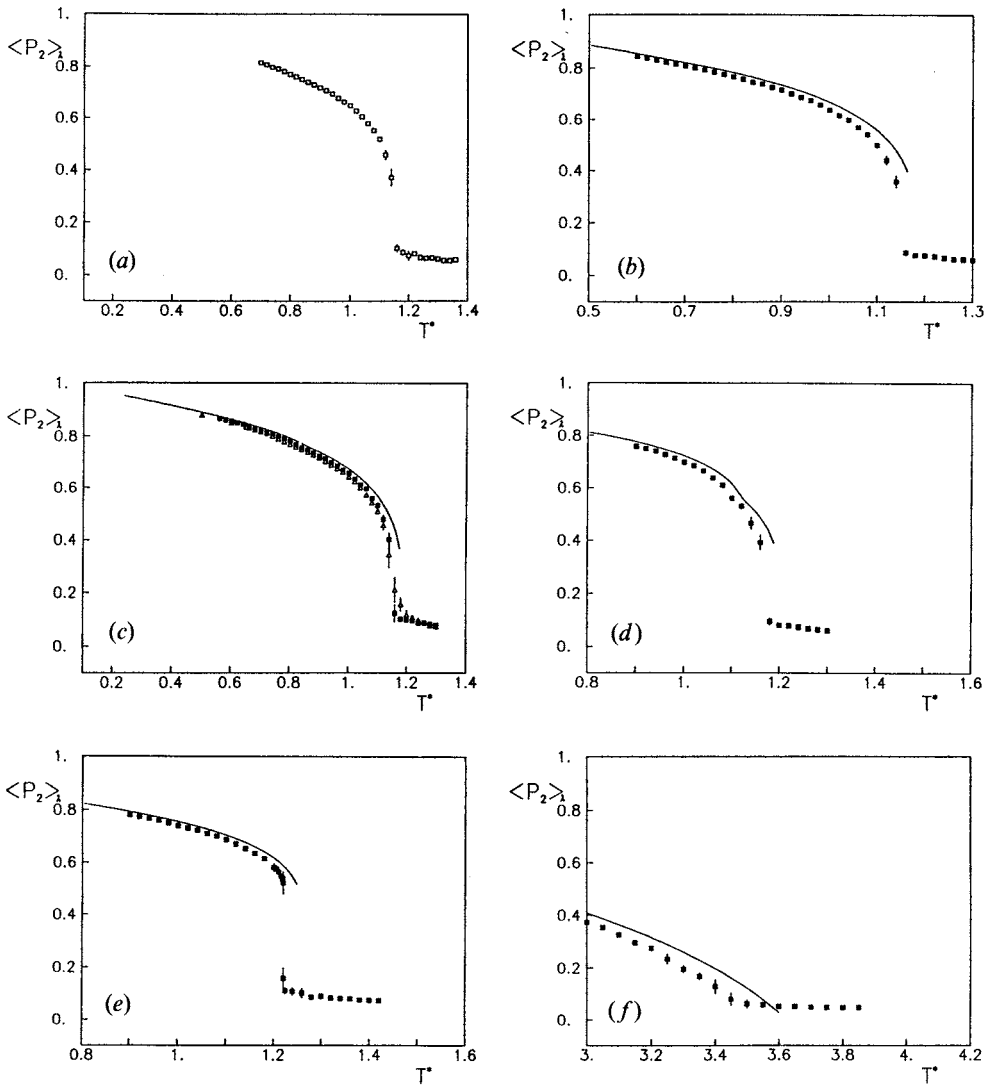

Figure 8. The second-rank order parameter, $\langle P_2 \rangle$ plotted against reduced temperature T^* obtained from CMC (■, □) at ξ (*c*) 0·2, (*e*) 0·4, (*f*) 2·0 (8 × 8 × 8 lattice) and ξ (*a*) −0·2, (*b*) 0·14, (*d*) 0·3 (10 × 10 × 10 lattice), from 10 × 10 × 10 PBMC (△) (only ξ = 0·2), and TSC theory (——).

only second rank properties are monitored. Indeed, the second-rank order parameter varies regularly until it drops to zero at the nematic–isotropic transition.

The general agreement between simulations and two-site cluster results is fairly good both for the transition location and for the temperature dependence of the order parameters. We do not show, for economy of space, results for the fourth-rank long range order parameters since they do not modify the overall picture. In figure 9 we show instead the first and second-rank short-range order parameters.

As already mentioned in section 2, these short-range order parameters correspond to the nearest-neighbour distance value of the pair distribution $G_L(r)$. σ_1 describes the

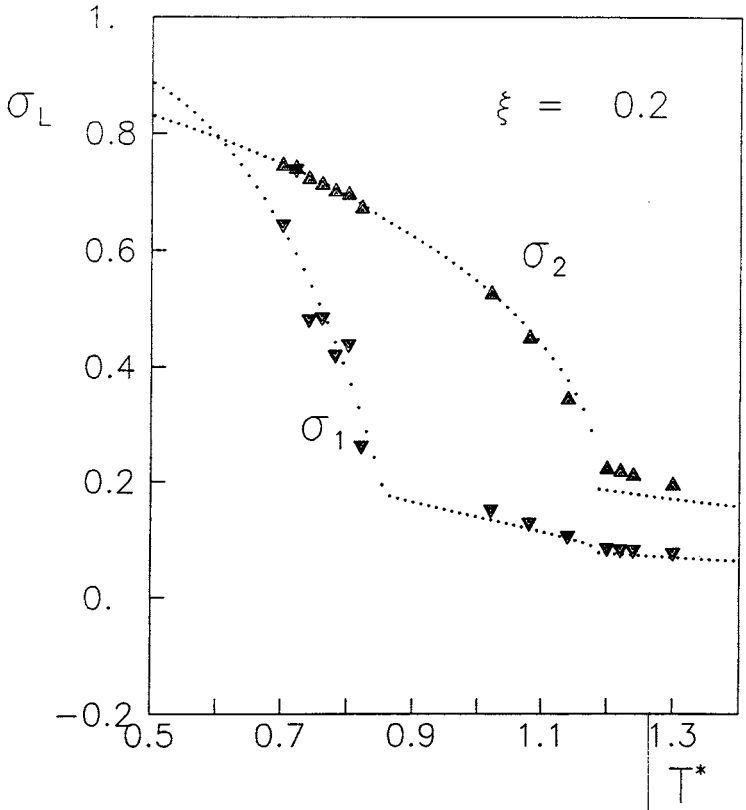

Figure 9. The first- and second-rank short range order parameters $\sigma_1 \equiv \langle \cos \beta_{12} \rangle$ and $\sigma_2 \equiv \langle P_2(\cos \beta_{12}) \rangle$ against reduced temperature T^* for $\xi = 0{\cdot}2$ as obtained from Monte Carlo simulation (symbols) and from two-site cluster (line). Notice that short-range polar order does not vanish in the nematic phase.

ability of a molecule to discriminate the sense of the orientation of its nearest neighbours. In figure 9 we show the temperature dependence of the $8 \times 8 \times 8$ CMC results compared with the TSC prediction (dotted line). The short range polar order is non zero in the nematic even though it is greatly reduced compared to the ferroelectric phase values. Computer simulations allow to calculate the full distance dependent pair correlation $G_L(r)$. In figure 10 we plot $G_1(r)$ and $G_2(r)$ together with the nearest-neighbour value from TSC at three different temperatures and for $\xi = 0{\cdot}2$. We also show, with a dashed line as a guide to the eye, the results for the antiferroelectric choice of ξ at the lowest temperature (cf. top left plate). In this case $G_1(r)$ oscillates, with the negative values corresponding to the probability of finding antiparallel molecular pairs.

5. Conclusions

We have shown that a simple combination of a second-rank aligning interaction and a first rank discriminating interaction simulating the head–tail asymmetry is sufficient to obtain a polar liquid crystal as well as a nematic phase. Dipolar forces do not have to be the interactions presiding to discrimination but rather this could be produced by other molecular mechanisms, as discussed in section 1. If, however, the

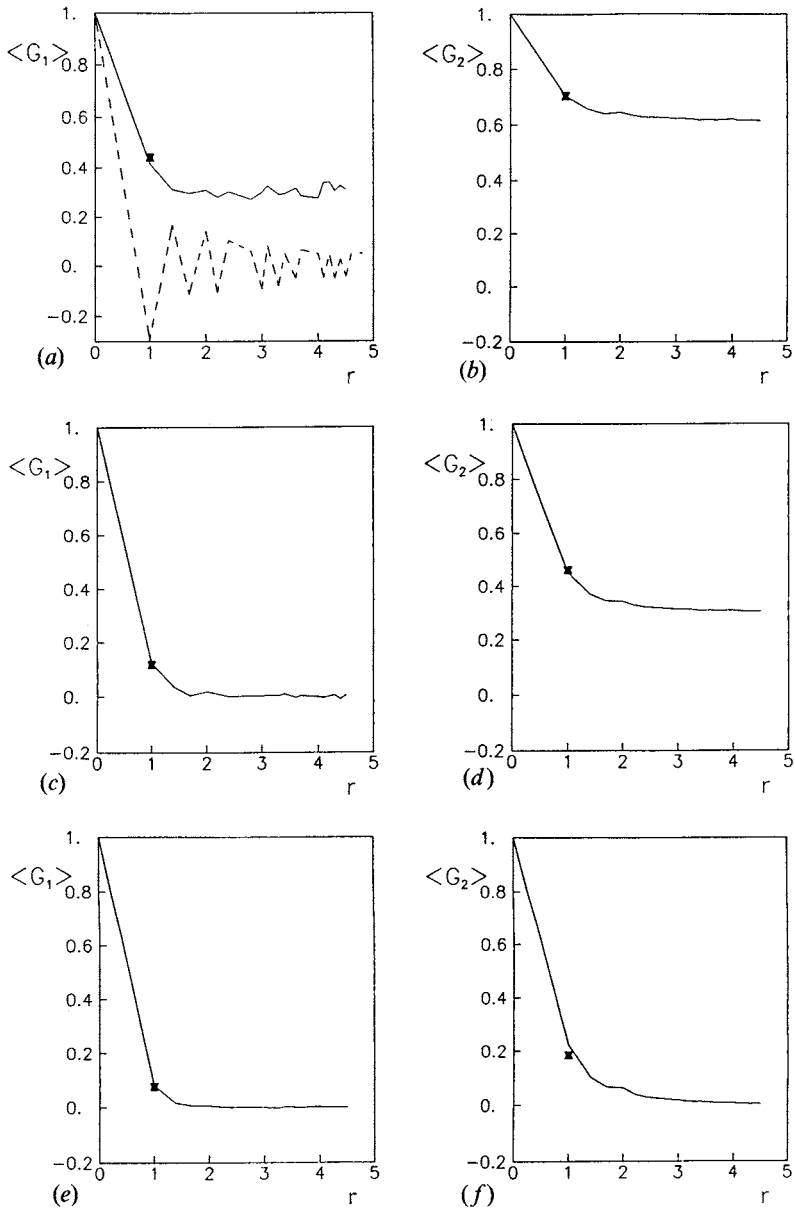

Figure 10. The first- and second-rank order short range correlation function $G_1(r) = \langle \cos \beta_{12} \rangle_r$ and $G_2(r) = \langle P_2(\cos \beta_{12}) \rangle_r$ against separation r in lattice units. Results for $\xi = 0{\cdot}2$ as obtained from CMC simulation at $T^* = 0{\cdot}78$, 1·080, 1·20 from top to bottom. A line through the points is drawn as a guide to the eye. We also report at $T^* = 0{\cdot}78$ $G_1(r)$ for $\xi = -0{\cdot}2$ (dashed line). The symbol is the two-site cluster result for nearest-neighbour separation.

molecules carry a dipole, the long-range order of the mesophase with $\langle P_1 \rangle \neq 0$ will provide ferroelectric behaviour. The polar mesophase either is the only ordered phase or, when the discriminating interactions are about 20% of the aligning ones, occurs at temperature of the order of 30% lower than that for the isotropic transition.

Attaching the mesogenic units as side groups in a polymer liquid crystal might be a way of reducing the change of crystallization and thus of observing the hitherto unobserved uniaxial ferroelecltric phase. Here we have shown that two-site cluster theory and Monte Carlo computer simulations basically support the phase diagram for the model obtained by Krieger and James, although significant quantitative differences are found. We have provided detailed results for first- and second-rank order parameters and for their temperature dependence that could in turn constitute the basis for predicting the relaxation properties of a uniaxial ferroelectric liquid crystal.

The simulations were performed on various clustered DEC VAXes and VAXstations at Dip. Fisica-INFN, Bologna and on a VAX and two VAXstations at Dip. Chimica Fisica. We wish to thank Consorzio INFM for financial support through Progetto Polimeri Liquid Cristallini. MPI and CNR are also thanked for supporting part of this work.

References

[1] Beresnev, L. A., Blinov, L. M., Osipov, M. A., and Pikin, S. A., 1988, *Molec. Crystals liq. Crystals*, **158A,** 3.
[2] Zentel, R., 1989, *Angew. Chem. Advanced Mater.*, **101,** 321.
[3] Vallerien, S. U., Kremer, F., Kapitza, H., Zentel, R., and Frank, W., 1989, *Phys. Lett. A*, **138,** 219.
[4] Tredgold, R. H., 1990, *J. Phys. D*, **23,** 119.
[5] Born, M., 1916, *Sitz. Phys. Math.*, **25,** 614.
[6] Chandrasekhar, S., 1977, *Liquid Crystals* (Cambridge University Press).
[7] Luckhurst, G. R., and Gray, G. W. (editors), 1979, *The Molecular Physics of Liquid Crystals* (Academic Press).
[8] Demus, D., 1989, *Liq. Crystals.*, **5,** 75.
[9] Luckhurst, G. R., and Zannoni, C., *Nature, Lond.*, **267,** 412.
[10] Madhusudana, N. V., and Chandrasekhar, S., 1975, *Pramana Suppl.*, **1,** 57.
[11] Madhusudana, N. V., Savithramma, K. L., and Chandrasekhar, S., 1977, *Pramana*, **8,** 22.
[12] Sarkar, S., and Tough, R. J. A., 1982, *J. Phys., Paris*, **43,** 1543.
[13] Dowell, F., 1985, *Phys. Rev. A*, **31,** 3214.
[14] Dunmur, D. A., and Toriyama, K., 1986, *Liq. Crystals*, **1,** 169.
[15] Indekeu, J. O., and Berker, A. N., 1986, *Physica*, **140A,** 368.
[16] Pershin, V. K., and Konoplev, V. A., 1986, *Soviet Phys. Tech. Phys.*, **31,** 456.
[17] Palffy-Muhoray, P., Lee, M. A., and Petschek, R. G., 1988, *Phys. Rev. Lett.*, **60,** 2303.
[18] Tiddy, G. J. T., 1980, *Phys. Rep.*, **57,** 2.
[19] Lei, Lin, 1987, *Molec. Crystals liq. Crystals*, **146,** 41.
[20] Leung, K. M., and Lei, Lin, 1987, *Molec. Crystals liq. Crystals*, **146,** 71.
[21] Malthête, J., and Collet, A., 1985, *Nouv. J. Chimie*, **9,** 151.
[22] Zimmermann, H., Poupko, R., Luz, Z., and Billard, J., 1985, *Z. Natur.*, **40a,** 149.
[23] Dalcanale, E., Bonsignore, S., Cometti, G., and Du Vosel, A., 1988, Italy Patent 21308 A/88.
[24] Ui, H., 1970, *Prog. Theor. Phys.*, **44,** 153.
[25] Derzhanski, A., and Petrov, A. G., 1982, *Molec. Crystals liq. Crystals*, **89,** 339.
[26] Lebwohl, P. A., and Lasher, G., 1972, *Phys. Rev. A*, **6,** 426.
[27] Krieger, T. J., and James, H. M., 1954, *J. chem. Phys.*, **22,** 796.
[28] Schoenmaker, B., and Ruijgrok, Th. W., 1988, *Physica A*, **153,** 372.
[29] Binder, K., editor, 1984, *Applications of the Monte Carlo Method in Statistical Physics* (Springer).
[30] Zannoni, C., 1979, *The Molecular Physics of Liquid Crystals*, edited by G. R. Luckhurst and G. W. Gray (Academic Press) p. 191.

[31] LUCKHURST, G. R., 1979, *The Molecular Physics of Liquid Crystals*, edited by G. R. LUCKHURST and G. W. GRAY (Academic Press) p. 85.
[32] CHICCOLI, C., PASINI, P., BISCARINI, F., and ZANNONI, C., 1988, *Molec. Phys.*, **65,** 1505.
[33] STRIEB, B., CALLEN, H. B., and HORWITZ, G., 1963, *Phys. Rev.*, **130,** 1798.
[34] VAN DER HAEGEN, R., DEBRUYNE, J., LUYCKX, R., and LEKKERKERKER, H. N. W., 1980, *J. chem. Phys.*, **73,** 2469.
[35] ROSE, M. E., 1957, *Elementary Theory of Angular Momentum* (Wiley).
[36] JAMES, F., and ROOS, M., 1971, MINUIT minimization package, CERN Library, D-506.
[37] FABBRI, U., and ZANNONI, C., 1986, *Molec. Phys.*, **58,** 763.
[38] ZANNONI, C., 1986, *J. chem. Phys.*, **84,** 424.
[39] LEVINE, R. D., and TRIBUS, M. (editors), 1979, *The Maximum Entropy Formalism* (MIT Press).
[40] 1982, *IMSL Library Reference Manual*, 9th edition (IMSL).
[41] ABRAMOWITZ, M., and STEGUN, I. A. (editors), 1964, *Handbook of Mathematical Functions* (Dover).
[42] BARKER, J. A., and WATTS, R. O., 1969, *Chem. Phys. Lett.*, **3,** 144.
[43] CHATFIELD, C., 1983, *Statistics for Technology* (Chapman and Hall), 3rd edition.
[44] FULLER, G., LUCKHURST, G. R., and ZANNONI, C., 1985, *Chem. Phys.*, **92,** 105.